High-K isomers in ^{176}W and mechanisms of K violation

B. Crowell,* P. Chowdhury,† D. J. Blumenthal,* S. J. Freeman,‡ and C. J. Lister*
Wright Nuclear Structure Laboratory, Yale University, New Haven, Connecticut 06511

M. P. Carpenter, R. G. Henry,§ R. V. F. Janssens, T. L. Khoo, T. Lauritsen, Y. Liang,‖ and F. Soramel¶
Argonne National Laboratory, Argonne, Illinois 60439

I. G. Bearden**
Purdue University, West Lafayette, Indiana 47907
(Received 6 February 1995)

An isomer, with $t_{1/2}=35\pm10$ ns and $J,K^{\pi}=14,14^{+}$, has been observed in the nucleus ^{176}W using the reaction ^{150}Nd(^{30}Si,4n) at a beam energy of 133 MeV. The isomer exhibits an unusual pattern of decay in which the *majority* of the flux proceeds directly to states with $\langle K\rangle=0$, bypassing available levels of intermediate K. This severe breakdown of normal K-selection rules in ^{176}W is compared with recent observations of K violation in neighboring nuclei, within the framework of proposed theoretical approaches. The available data on these K-violating decays seem to have a consistent explanation in models of K mixing which include large-amplitude fluctuations of the nuclear shape.

PACS number(s): 23.20.Lv, 21.10.Re, 21.60.Ev, 27.70.+q

I. INTRODUCTION

A quantum-mechanical system containing a finite number of particles can often be accurately described in terms of a shape. For particles moving in a mean field imposed by such a shape, symmetries of the shape imply the existence of conserved quantum numbers. In deformed nuclei with axially symmetric equilibrium shapes, the projection K of the total angular momentum along the axis of symmetry is an example of such an approximately conserved quantum number. The yrast states (i.e., the states with the lowest energy for a given angular momentum) in even-even nuclei with such shapes are most commonly those involving collective rotation, with $K=0$. Collective rotation does not contribute to K, because a quantum rotor cannot rotate about an axis of symmetry. High-K states compete with collective rotation as an energy-efficient mode of accommodating angular momentum only in a small number of nuclei near $A=180$. These nuclei have many orbitals near the neutron and proton Fermi surfaces with large projections Ω of the individual nucleonic angular momenta along the axis of symmetry.

Systematic studies have revealed a normal pattern of decay of high-K states which proceeds stepwise to lower values of K, minimizing ΔK at each step [1]. When the only available decay mode is via a transition with a large ΔK, the decay is hindered and the level is isomeric. The existence of such isomers, known as K isomers, is a clear indication of the approximate conservation of the K quantum number. The associated selection rule involves the degree of K forbiddenness, ν, defined as $\nu=|\Delta K|-\lambda$, where λ is the multipolarity of the gamma-ray transition associated with the decay. Thus, ν denotes the part of ΔK that cannot be accounted for by the angular momentum carried away by the photon. Transitions with $\nu>0$ are forbidden to first order and are hindered. A high-K isomer is able to decay to a state of lower K only because of very small admixtures of nondominant values of K in the wave functions of the initial or final state, or both. An empirical measure of K mixing is the hindrance factor $F=t_{1/2}/t_{1/2}^{W}$, where $t_{1/2}$ is the experimentally determined partial half-life of the transition and $t_{1/2}^{W}$ is the Weisskopf estimate for the half-life of a single-particle transition. The typical observation is that F increases by a factor of about 100 per degree of K forbiddenness [2].

One mechanism that has clearly been shown to contribute to K mixing, especially for small values of ΔK, is Coriolis mixing with a fixed shape [1]. This represents fluctuations in the angle between the axis of symmetry and the angular momentum vector. In the rotating body-fixed frame, the Coriolis force contributes to the Hamiltonian a term $H_{\mathrm{Cor}}=-\omega J_x$, where ω is the rotational frequency and J_x is the component of the angular momentum perpendicular to the axis of symmetry. The matrix elements of H_{Cor} link states differing by $\Delta K=\pm1$, and are typically small compared to the spacing of states with a given K value, so that a perturbative treatment of the mixing converges rapidly. Coriolis admixtures with large ΔK occur only in high-order perturbation theory, and should show a roughly exponential increase of F as a function of ν. This is precisely what was observed in all the cases originally studied [2], and until recently, the physical mecha-

*Present address: Argonne National Laboratory, Argonne, IL 60439.
†Present address: Dept. of Physics, Univ. of Massachusetts Lowell, Lowell, MA 01854.
‡Present address: Schuster Laboratory, University of Manchester, Manchester M13 9PL, United Kingdom.
§Present address: Dept. of Radiology, University of California at San Francisco, San Francisco, CA 94143.
‖Present address: Dept. of Radiology, Indiana Univ. Medical Center, Indianapolis, IN 46202.
¶Present address: Present address: Dept. of Physics, University of Udine, I-33100 Udine, Italy; on leave from Universitá di Padova, Padova, Italy.
**Present address: Niels Bohr Institute, DK-4000 Roskilde, Denmark.

nisms of K mixing were thought to be fairly well understood in terms of Coriolis couplings.

More recently, transitions with large ΔK, but abnormally low hindrance factors, have been observed in a few nuclei [3–5]. This constitutes a challenge to the established picture of Coriolis mixing. A new mechanism that has been suggested to explain these abnormal cases [3,6] involves large-amplitude quantum fluctuations of the shape away from axial symmetry, measured by the triaxiality parameter γ. Small nonaxial ellipsoidal fluctuations cause $\Delta K = \pm 2$ mixing, and can therefore only cause large-ΔK admixtures through higher-order effects. Large nonaxial fluctuations, however, may result in a complete rearrangement of the nuclear wave function, and cannot be understood perturbatively. Such fluctuations could carry a nucleus from $\gamma = -120°$ (an axially symmetric prolate shape with $K = J$) to $\gamma = 0°$ (the same shape with $K = 0$), penetrating a barrier in the potential at intermediate values of γ [3,6]. Such a mechanism is referred to as γ tunneling. The definition of γ adopted here corresponds to the Lund convention.

Our goal in this work was to find experimental observations and theoretical methods that would allow a comparison of simple models of γ tunneling and Coriolis mixing as descriptions of these anomalous decays of K isomers. If γ tunneling is an important mechanism in these anomalous decays, then the measured hindrance factors should vary strongly as a function of the shape and height of the potential barrier between the minima at $\gamma = -120°$ and $\gamma = 0°$. In the $A \sim 180$ region, the height of this barrier is predicted to vary rapidly with changing proton number, based on calculations of the potential energy surfaces described in Sec. IV. In agreement with these calculations, the measured excitation energies of γ-vibrational bands also show significant changes [7], reflecting variations in the softness towards triaxial deformations. If Coriolis mixing is the dominant mechanism, then the strengths of the decays should be a function of variables such as the quasiparticle (qp) configuration, the deformation, and the rotational frequency, and should not depend on the shape of the potential energy surface.

The nucleus ^{176}W is a good candidate for testing these models. It is an isotone of ^{174}Hf, in which weak branches with large ΔK have been observed [4] in the decay of a $K = 14$ isomer, competing with stronger branches having small ΔK. An investigation of the decay modes of isomers in ^{176}W at similar spins allows a comparison of these two isotones within the framework of the proposed models. This paper presents the results of a detailed experimental study of both the delayed and prompt gamma decay of ^{176}W, including the observation of an isomer with an unusual pattern of decay. The broad spectroscopic information contributes vitally to the understanding of the physics of K isomers by identifying many of the low-lying intrinsic structures which are the building blocks for the multiquasiparticle K isomers, and by mapping out, as completely as possible, the set of levels available for the decay of the K isomers. Calculations are also performed and compared with the experimental data. Partial results of this work have been reported previously [8].

II. SPECTROSCOPY OF ^{176}W

A. Experiment

The experiment was carried out at the ATLAS facility at Argonne National Laboratory using the reaction ^{150}Nd(^{30}Si,4n) at a beam energy of 133 MeV. The target consisted of 1.1 mg/cm^2 of isotopically pure ^{150}Nd on a 53 mg/cm^2 Pb backing, with a thin layer of Au evaporated on the front of the target to prevent oxidation. The intrinsic timing characteristics of the accelerator system provided pulses of <1 ns duration, separated by 82 ns. The gamma rays were detected by the Argonne-Notre Dame BGO gamma-ray facility [9], which consists of 12 Compton-suppressed Ge detectors and an inner array of 50 BGO elements. The master trigger for the experiment required two Compton-suppressed Ge detectors to fire within 120 ns of each other, in coincidence with at least four BGO detectors. In all, 45×10^6 events were recorded.

In order to extract information on weakly populated K isomers, the data from the BGO detectors were recorded and analyzed in more detail than is usually required in studies of high-spin states. The energy and time parameters of each individual BGO element were written to tape on an event-by-event basis, in addition to the usual energy and time parameters of the Ge detectors. All times were measured relative to the radio-frequency signal from the accelerator, which is related to the time of arrival of the beam pulse at the target. The terms ''prompt'' and ''in-beam'' will be used interchangeably to indicate gamma-ray transitions occurring during a beam burst (as defined by the timing resolution of the detectors).

The energy and timing information from the BGO detectors was used to create several data sets of Ge-Ge coincidences with different coincidence requirements. In addition to the normal BGO fold (i.e., the number of BGO elements that fired within the coincidence window) and BGO sum energy parameters, a delayed BGO fold parameter was created, defined as the number of BGO elements that fired between beam bursts. This provided an extremely sensitive and efficient coincidence trigger for isolating decays of high-spin isomers. Gamma-gamma coincidence matrices were constructed with requirements on both total and delayed BGO fold in order to enhance coincidences above, below, and across the isomers.

Spectroscopy of isomers requires an accurate determination of the timing of the detected gamma rays. In addition, an accurate measurement of the intensity of both prompt and delayed gamma rays is extremely sensitive to the requirements on the time parameters. Therefore, these parameters need special attention in order to correct for the intrinsic changes in timing of the Ge and BGO detectors with variations in gamma-ray energy. Constant-fraction discriminators (CFD's), which were used for both Ge and BGO timing, provide a first-order correction for the dependence of the timing signal on the amplitude of the pulse from the detector. In practice, however, variations as a function of energy are observed, both in the mean timing and the timing resolution, due to the inherent physics of the detector's operation. This effect is not automatically corrected for in an efficiency calibration using radioactive sources, for which there is no timing reference and therefore no time parameter. Incorrect gamma-ray intensities will be extracted from coincidence data if no correction is made. The timing parameters for both BGO and Ge detectors were therefore adjusted off line according to the empirical formula $t \rightarrow t + aE_\gamma^b$, where a and b were fit to the data. When setting a coincidence condition

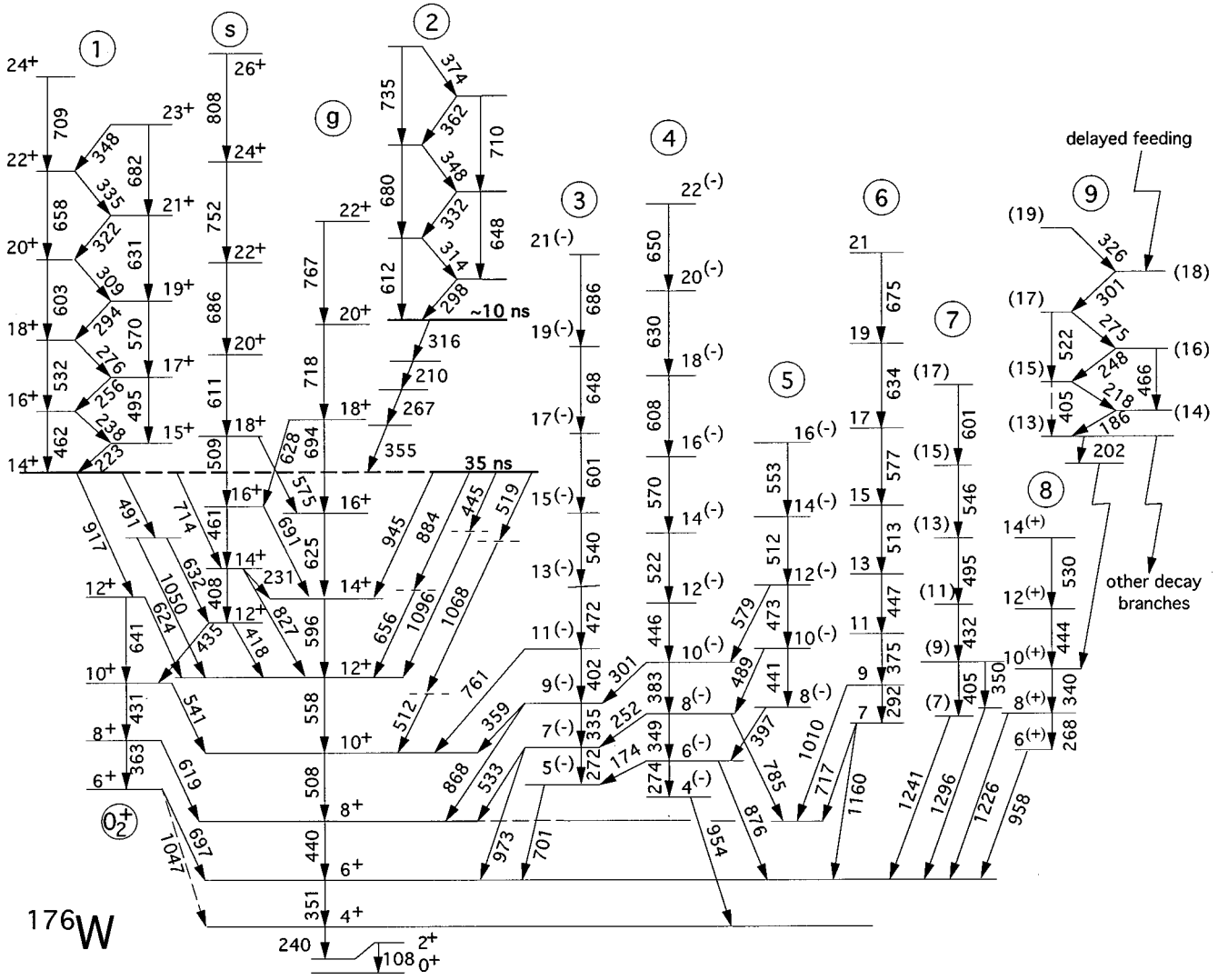

FIG. 1. Level scheme of ^{176}W deduced from this work. Gamma-ray transitions are shown with their energies in keV, and states with their spin and parity. The labels for the rotational bands are shown in circles above or below the bands (see text).

around the prompt peak at t_0 in the Ge time spectra, it was necessary as well to vary the width of the coincidence window (and the width of the window for subtracting random coincidences) to accept a fixed fraction of the peak, regardless of energy. The observed widths of the peaks in the time spectra, as a function of energy, were fitted to the functional form $w_t = cE_\gamma^d$, and the widths of the time windows were set accordingly as a function of energy, usually to cover the range of $t_0 \pm 1.7\sigma$, where σ denotes the standard deviation.

B. Level scheme

The complete decay scheme of ^{176}W derived in this experiment is shown in Fig. 1. It includes 148 transitions, about a factor of 4 more than reported in earlier work [10,11]. The energies and intensities of the observed gamma rays are given in Table I, along with the spin assignments of the relevant levels. The intensity of the weakest gamma ray recorded in the table is about 0.025% of the total population of ^{176}W, corresponding to an absolute cross section of ~ 5 μb. Twelve rotational bands are observed (Fig. 1), of which eight are new in this work. The bands with $K>0$ are labeled in the level scheme by numbers from 1 to 9 to facilitate discussion in the text. The ground-state band (states involving only collective rotation) is referred to as the g band, the lowest configuration containing two rotation-aligned neutrons as the s band, and the band built on the first excited $K^\pi = 0^+$ state as the 0_2^+ band. The spins of the levels observed in this work were deduced by the method of directional correlations from oriented states (DCO's), with the DCO ratios defined as in Ref. [9]. These ratios are given below where they are relevant for determining the spins of the various bandheads. Quadrupole transitions were found to have DCO ratios clustered around 0.95, and dipoles around 0.45. A more complete list of DCO ratios is given in Ref. [12]. The observation of regular rotational cascades of $M1$ and $E2$ transitions throughout the level scheme served as an additional check on the consistency of the spin assignments. In the following two subsections, the level scheme is separately discussed for (i) the $K=0$ and intermediate-K states primarily observed in the prompt spectroscopy and (ii) the feeding and decay of high-K isomers.

TABLE I. Energies and intensities of gamma rays in ^{176}W observed in this work, and spin assignments (from measured DCO ratios) for the initial and final states of the transitions.

E_γ (keV)	I_γ [a]	$K,J^\pi \rightarrow K,J^\pi$		E_γ (keV)	I_γ [a]	$K,J^\pi \rightarrow K,J^\pi$	
107.8(1)	25 [b]	$0_g,2^+$	$0_g,0^+$	405.4(3)	0.7(2)	(7,9)	(7,7)
174.2(3)	0.6(1)	$4,6^{(-)}$	$4,5^{(-)}$	408.4(1)	2.8(2)	$0_s,14^+$	$0_s,12^+$
186.3(2)	0.7(2)	(13,14)	(13,13)	418.0(1)	2.0(6)	$0_s,12^+$	$0_s,12^+$
202.1(6)	~0.1	c		430.8(2)	0.9(2)	$0_2,10^+$	$0_2,8^+$
210.5(1)	0.07[d]	e		431.6(3)	1.3(2)	(7,11)	(7,9)
218.0(4)	0.5(2)	(13,15)	(13,14)	434.7(1)	2.3(2)	$0_s,12^+$	$0_2,10^+$
219.0(4)	0.6(2)	f		440.4(1)	56(2)	$0_g,8^+$	$0_g,6^+$
222.8(1)	1.1(2)	$14,15^+$	$14,14^+$	441.0(3)	1.8(4)	$8,10^{(-)}$	$8,8^{(-)}$
230.7(1)	1.0(2)	$0_s,14^+$	$0_g,14^+$	443.7(1)	0.7(3)	$6,12^{(+)}$	$6,10^{(+)}$
238.2(1)	0.9(2)[d]	$14,16^+$	$14,15^+$	445(1)	0.25(6)[i, j]	k	
239.7(1)	82(6)	$0_g,4^+$	$0_g,2^+$	445.5(1)	4.4(2)	$4,12^{(-)}$	$4,10^{(-)}$
247.7(2)	0.6(2)	(13,16)	(13,15)	446.7(1)	3.0(2)	(7,13)	(7,11)
251.9(3)	0.5(1)	$4,8^{(-)}$	$4,7^{(-)}$	460.9(1)	1.8(4)	$0_s,16^+$	$0_s,14^+$
256.2(1)	0.6(1)[d]	$14,17^+$	$14,16^+$	461.7(2)	0.27(5)[d]	$14,16^+$	$14,14^+$
266.6(1)	0.44(8) [d]	e		466.5(5)	0.2(2)	(13,16)	(13,14)
267.6(2)	0.8(1)	$6,8^{(+)}$	$6,6^{(+)}$	472.1(1)	6.0(2)	$4,13^{(-)}$	$4,11^{(-)}$
272.3(1)	0.6(1)	$4,7^{(-)}$	$4,5^{(-)}$	473.1(3)	1.6(3)	$8,12^{(-)}$	$8,10^{(-)}$
273.9(1)	3.0(2)	$4,6^{(-)}$	$4,4^{(-)}$	489.0(3)	1.1(3)	$8,10^{(-)}$	$4,8^{(-)}$
275.0(2)	0.6(2)	(13,17)	(13,16)	490.9(2)	0.4(1)[i,j]	k	
275.9(1)	0.5(1)[d]	$14,18^+$	$14,17^+$	494.8(3)	1.0(2)	(7,13)	(7,11)
292.0(1)	1.3(1)	(7,9)	(7,7)	494.9(1)	0.39(5)[d]	$14,17^+$	$14,15^+$
293.5(1)	0.3(1)[d]	$14,19^+$	$14,18^+$	508.4(1)	46(2)	$0_g,10^+$	$0_g,8^+$
297.8(1)	0.20(4)	g		508.8 [l]	1.8(5)	$0_s,18^+$	$0_g,16^+$
300.6(3)	0.4(1)	$4,10^{(-)}$	$4,9^{(-)}$	512.2(3)	2.0(4)	$8,14^{(-)}$	$8,12^{(-)}$
301.3(3)	0.5(1)	(13,18)	(13,17)	512.2(3)	0.05(3)[i,j]	k	
308.6(1)	0.3(1)[d]	$14,20^+$	$14,19^+$	513.4(1)	2.8(5)	(7,15)	(7,13)
313.7(1)	0.23(5) [d]	g		518.6(3)	0.29(6)[i,j]	k	
315.8(1)	0.28(6) [d]	e		522.1(1)	3.2(2)	$4,14^{(-)}$	$4,12^{(-)}$
322.4(2)	h	$14,21^+$	$14,20^+$	522.5(5)	0.3(2)	(13,17)	(13,15)
326.0(4)	0.3(1)	(13,19)	(13,18)	530.5(2)	0.5(3)	$6,14^{(+)}$	$6,12^{(+)}$
331.7(1)	0.27(5) [d]	g		532.5(1)	0.46(6)[d]	$14,18^+$	$14,16^+$
334.6(1)	3.4(2)	$4,9^{(-)}$	$4,7^{(-)}$	533.1(1)	2.6(4)	$4,7^{(-)}$	$0_g,8^+$
334.8(4)	0.11(4) [d]	$14,22^+$	$14,21^+$	540.4(1)	4.6(3)	$4,15^{(-)}$	$4,13^{(-)}$
339.8(2)	0.6(1)	$6,10^{(+)}$	$6,8^{(+)}$	541.1(1)	1.0(2)	$0_2,10^+$	$0_g,10^+$
347.6(3)	h	g		545.7(3)	0.6(2)	(7,15)	(7,13)
348.2(2)	h	$14,23^+$	$14,22^+$	553.3(3)	0.8(2)	$8,16^{(-)}$	$8,14^{(-)}$
348.8(1)	5.5(3)	$4,8^{(-)}$	$4,6^{(-)}$	557.8(1)	28(2)	$0_g,12^+$	$0_g,10^+$
350		(7,9)		569.8(1)	1.3(3)	$4,16^{(-)}$	$4,14^{(-)}$
350.8(1)	79(2)	$0_g,6^+$	$0_g,4^+$	569.8(2)	0.38(5)[d]	$14,19^+$	$14,17^+$
354.6(1)	0.8(2)[d]	e		574.7(1)	4.0(6)	$0_s,18^+$	$0_g,16^+$
359.0(3)	0.7(1)	$4,9^{(-)}$	$0_g,10^+$	576.7(1)	2.6(6)	(7,17)	(7,15)
362.1(3)	h	g		579.1(5)	0.4(1)	$8,12^{(-)}$	$4,10^{(-)}$
363.0(2)	0.5(1)	$0_2,8^+$	$0_2,6^+$	595.9(1)	19(1)	$0_g,14^+$	$0_g,12^+$
374.0(3)	0.19(4) [d]	g		600.7(5)	0.6(2)	(7,17)	(7,15)
374.6(1)	2.9(2)	(7,11)	(7,9)	600.8(1)	3.1(4)	$4,17^{(-)}$	$4,15^{(-)}$
382.8(1)	4.1(3)	$4,10^{(-)}$	$4,8^{(-)}$	603.0(2)	0.37(6)[d]	$14,20^+$	$14,18^+$
397.0(3)	0.7(2)	$8,8^{(-)}$	$4,6^{(-)}$	607.7(1)	1.0(1)	$4,18^{(-)}$	$4,16^{(-)}$
401.6(1)	5.5(3)	$4,11^{(-)}$	$4,9^{(-)}$	611.0(1)	3.0(5)	$0_s,20^+$	$0_s,18^+$
405.0(3)	<0.1	(13,15)	(13,13)				

TABLE I. (*Continued*).

E_γ (keV)	I_γ [a]	$K,J^\pi \rightarrow K,J^\pi$		E_γ (keV)	I_γ [a]	$K,J^\pi \rightarrow K,J^\pi$	
612.0(4)	0.27(5)[d]	g		718.3(3)	1.5(4)	$0_g,20^+$	$0_g,18^+$
618.8(2)	1.4(4)	$0_2,8^+$	$0_g,8^+$	735.0(5)	h	g	
624.0(4)	1.0(4)	$0_2,12^+$	$0_g,12^+$	752.1(2)	0.4(1)	$0_s,24^+$	$0_s,22^+$
625.3(1)	8.8(6)	$0_g,16^+$	$0_g,14^+$	760.9(1)	1.6(3)	$4,11^{(-)}$	$0_g,10^+$
628.0(5)	1.6(3)	$0_g,18^+$	$0_s,16^+$	767.3(4)	0.5(2)	$0_g,22^+$	$0_g,20^+$
629.7(2)	0.7(1)	$4,20^{(-)}$	$4,18^{(-)}$	785.4(1)	1.1(1)	$4,8^{(-)}$	$0_g,8^+$
631.1(2)	0.29(6)[d]	$14,21^+$	$14,19^+$	808(1)	0.3(1)	$0_s,26^+$	$0_s,24^+$
632(1)	0.07(4)[i,j]	k		826.6(1)	0.8(1)	$0_s,14^+$	$0_g,12^+$
633.9(1)	1.2(2)	(7,19)	(7,17)	866 [m]	<0.2	$14,14^+$	$4,13^{(-)}$
641.2(2)	0.5(2)	$0_2,12^+$	$0_2,10^+$	867.8(1)	3.0(4)	$4,9^{(-)}$	$0_g,8^+$
647.9(4)	0.18(4)[d]	g		876.4(1)	5(2)	$4,6^{(-)}$	$0_g,6^+$
648.0(2)	1.2(2)	$4,19^{(-)}$	$4,17^{(-)}$	884.5(2)	0.25(6)[i]	k	
650.0(1)	0.4(1)	$4,22^{(-)}$	$4,20^{(-)}$	916.8(3)	0.31(4) [i]	$14,14^+$	$0_2,12^+$
656.3(2)	0.25(6)[i,j]	k		945.0(2)	0.15(4) [i]	$14,14^+$	$0_g,14^+$
657.6(3)	0.26(6)[d]	$14,22^+$	$14,20^+$	953.7(1)	2.7(2)	$4,4^{(-)}$	$0_g,4^+$
674.7(1)	0.7(1)	(7,21)	(7,19)	957.6(1)	1.2(1)	$6,6^{(+)}$	$0_g,6^+$
680.2(4)	h	g		973.4(2)	2.2(4)	$4,7^{(-)}$	$0_g,6^+$
682.0(4)	h	$14,23^+$	$14,21^+$	1010.0(3)	1.2(1)	7,9	$0_g,8^+$
685.5(2)	2.1(7)	$0_s,22^+$	$0_s,20^+$	1047(1)	0.6(3)	$0_2,6^+$	$0_g,4^+$
685.7(3)	0.4(1)	$4,21^{(-)}$	$4,19^{(-)}$	1049.8(3)	0.21(6)[i,j]		$0_g,12^+$
691.2(3)	3.3(3)	$0_s,16^+$	$0_g,14^+$	1067.9(3)	0.16(6)[i,j]	k	
693.7(3)	2.7(3)	$0_g,18^+$	$0_s,16^+$	1096(1)	0.08(3)[i,j]	k	
697.0(2)	1.4(2)	$0_2,6^+$	$0_g,6^+$	1122 [m]	$<\sim 0.1$[j]	$14,14^+$	$0_s,12^+$
701.4(1)	2.2(6)	$4,5^{(-)}$	$0_g,6^+$	1159.5(4)	0.3(1)	7,7	$0_g,6^+$
708.6(4)	0.25(6)[d]	$14,24^+$	$14,22^+$	1225.9(1)	3.2(6)	$6,8^{(+)}$	$0_g,6^+$
709.5(4)	0.24(5)[d]	g		1240.6(3)	0.7(2)	(7,7)	$0_g,4^+$
714.1(1)	0.8(1)[i]	$14,14^+$	$0_s,14^+$	1296.4(3)	0.9(2)		$0_g,6^+$
717.4(4)	0.5(1)	(7,7)	8^+	1541 [m]	<0.06	$14,14^+$	$0_g,12^+$

[a]Intensities normalized to total intensity (gamma plus internal conversion) of the 108 keV transition (100%). All intensities are from coincidence spectra, with conditions on the number of detectors firing (at least two Ge detectors and ten BGO detectors).

[b]Based on theoretical internal conversion coefficient.

[c]Transition in cascade connecting band 9 to band 8.

[d]Intensity from a coincidence spectrum with conditions that both Ge detectors fire in beam and at least three BGO detectors fire out of beam, and normalized using intensity of the 223 keV transition.

[e]Transition in cascade connecting the 10-ns isomer to the 35-ns isomer.

[f]Decay transition of band 9, not placed in level scheme.

[g]Transition in band 2 built on 10-ns isomer.

[h]Not measurable.

[i]Intensity from a coincidence spectrum with conditions that both Ge detectors as well as at least two BGO detectors fire out of beam, and normalized using the intensity of the 35-ns isomer.

[j]The intensity listed is the intensity of population through the 35-ns isomer; the intensity due to prompt feeding could not be measured.

[k]Transition observed in the decay of the 35-ns isomer.

[l]Energy from sums and differences of other gamma-ray energies, and not determined directly from the centroid of a gamma-ray peak in a spectrum.

[m]Unobserved transition. An upper limit on the intensity was extracted to allow the calculation of a lower limit on the corresponding hindrance factor.

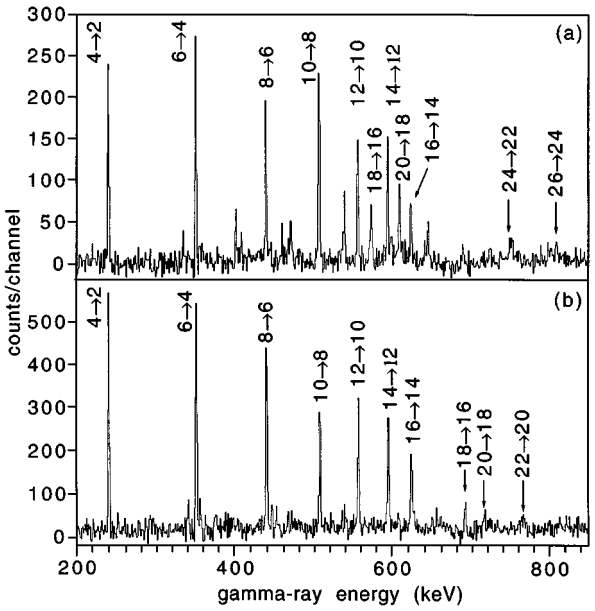

FIG. 2. Sample gamma-ray spectra for the $K=0$ states: (a) spectrum in coincidence with the 686 keV $22^+ \rightarrow 20^+$ transition, showing the high-spin s band; (b) sum of spectra in coincidence with the 694, 718, and 767 keV members of the nonyrast part of the g band. Both spectra have the additional coincidence requirement of BGO fold $\geqslant 10$.

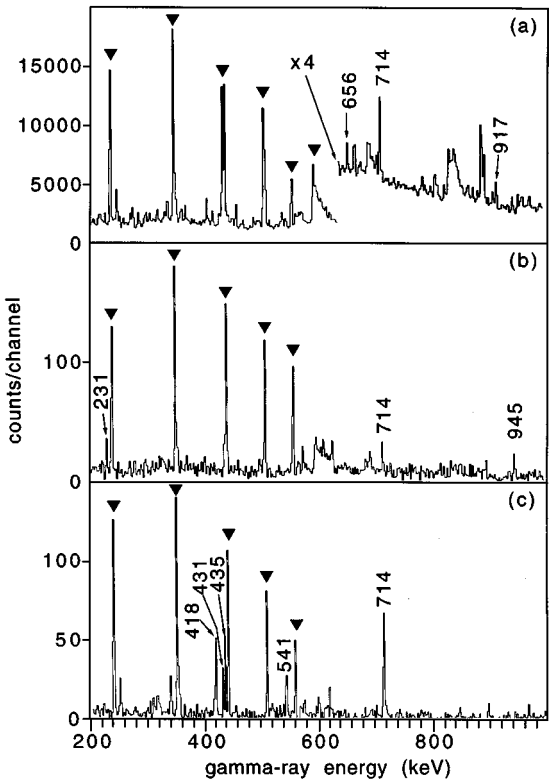

FIG. 3. Gamma-ray spectra based on coincidence events in which both Ge detectors registered delayed gamma rays: (a) total projection, (b) spectrum in coincidence with the 596 keV g-band transition, (c) spectrum in coincidence with the 408 keV transition from the s band. All spectra have the additional coincidence requirement of delayed BGO fold $\geqslant 1$. Transitions involved in the decay of the 35-ns isomer are labeled in keV. Transitions in the g band populated by the decay of the isomer are marked with triangles.

1. $K=0$ and intermediate-K states

The yrast s-band states in ^{176}W were extended to $J^\pi = 26^+$. The g band was also extended beyond the backbend to spin 22, and is discussed in more detail below. Many weakly populated, nonyrast structures were first noticed in this experiment because they were fed preferentially by the decay of high-spin isomers. The study of these structures probably would not have been possible with prompt spectroscopy alone. For example, a large number of nonyrast levels of the g, s, and 0_2^+ bands (Fig. 1) was first observed via decay of the 14^+ isomer. These nonyrast structures were then extended in prompt spectroscopy. Representative gamma-ray spectra for the g- and s-band states are shown in Fig. 2. The observation of the nonyrast members of the g band and s band is noteworthy, not just because these states are rarely observed, but also because of their relevance for understanding the highly K-violating decays. In particular, detailed spectroscopy of these bands in the region where they cross and interact allows the extraction of a matrix element for the interaction, and, as discussed in Sec. IV, this has important implications for testing the role of Coriolis mixing in the decay of high-K states to the g and s bands.

The spins of the various $K=0$ and intermediate-K rotational bands are all unambiguously determined, except for band 7, where the DCO ratio of 0.7(1) for the 1241 keV transition is not conclusive. The other two newly observed 2qp configurations are the bandheads of bands 5 and 6, whose spins are determined from the DCO ratios of 1.3(2) and 0.4(1), respectively, extracted for the 397 and 1010 keV transitions. The tentative parity assignments of bands 5 and 8 are based on the observation of fast quadrupole transitions linking states in these bands to structures with significantly different values of K. If these (K-violating) transitions were of $M2$ character, unprecedentedly low hindrance factors would be implied (e.g., $F \leqslant 1$ for the 397 keV transition depopulating band 5, compared to 10^6–10^{10} for a typical $M2$ transition with $\nu=6$ [2]). The negative parity tentatively assigned to band 3 (and, consequently, to its signature partner, band 4) is based on systematics. This parity assignment is also natural in view of the pattern of decay of band 3 to the g band, in which no quadrupole transitions are observed. For the 397–441 keV sequence near the bottom of band 5, the proposed ordering of transitions is based on the rotational pattern of levels. In the level scheme given in Ref. [12], the decay of band 7 to the g band is found to be incorrect based on more recent data from the GAMMASPHERE spectrometer, and has been corrected here. A more complete description of the results of the GAMMASPHERE experiment will be presented in a future paper.

2. Feeding and decay of high-K isomers

Two new high-spin isomers were observed in ^{176}W (Fig. 1). The more strongly populated one, for which complete patterns of feeding and decay were established, is assigned $K^\pi = 14^+$ for reasons explained below. Delayed feeding of yrast states, pointing to the existence of such an isomeric level in ^{176}W, had previously been reported [10]. An indica-

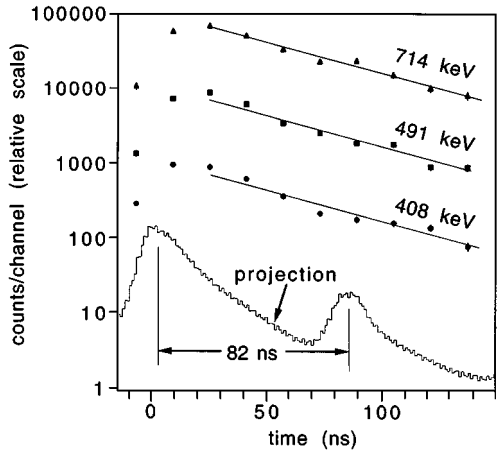

FIG. 4. Measurement of the half-life of the 35-ns isomer from the reaction ^{50}Ti(^{130}Te,4n) with a recoil-shadow geometry (see text). Three time spectra are shown, based on background-subtracted slices taken from a histogram of gamma-ray energy versus time. All times were measured relative to the rf pulse from the accelerator, which relates to the time of arrival of the beam. The lines through the data all show half-lives of 35 ns, with amplitudes fitted individually to the three spectra. The calibration of the time axis can be read directly from the total projection at the bottom, which shows the 82-ns beam-pulsing period of the accelerator. The data have been renormalized by factors of 100, 14, 1, and 1/2000, respectively, for the 714, 491, and 408 keV slices and the total projection.

tion of the quality of the data can be gained from the spectra in Fig. 3. The decay of the isomer, with a measured half-life of $t_{1/2}=35\pm10$ ns, includes a strongly K-violating branch, connecting the isomer directly to the 14^+ member of the ground-state band, as well as other direct branches to levels with $K=0$. In a previous description of this work [8], the half-life of this isomer was stated as $\sim$70 ns. An accurate measurement of the half-life was difficult in this experiment, since it was not possible to use the delayed BGO fold parameter to enhance the peaks whose half-lives were being fitted, since this would have introduced a bias in the time of the decay. In a more recent experiment using the reaction ^{50}Ti(^{130}Te,4n) and a recoil-shadow geometry [13], the Ge detectors were shielded from gamma rays emitted directly from the target, but were able to detect transitions emitted from recoiling ^{176}W nuclei that stopped in a Pb catcher foil 17 cm downstream. An event was collected if two Ge detectors and two BGO detectors registered signals in coincidence. Consequently, the peak-to-background ratios of the transitions depopulating the isomer were enhanced by more than an order of magnitude without any use of the delayed BGO fold parameter, thus allowing a much more reliable determination of the half-life, as shown in Fig. 4. The most significant cause of deviations from the fits lies in the systematic error in choosing the correct amount of background subtraction for the relevant gamma-ray peak. Other effects, such as the presence of later beam pulses and the feeding of the 35-ns isomer by a higher-lying isomer, are less significant. Despite these uncertainties, the half-lives extracted from the 714, 491, and 408 keV transitions, as shown in Fig. 4, as well as the 558, 440, and 917 keV transitions, all cluster around a value of 35 ns, within the present error bars of ±10 ns. Table II gives the intensities of the transitions depopulating the 35-ns isomer.

TABLE II. Intensities of transitions associated with the decay of the 35-ns isomer, listed as percentages of the total flux through the isomer (100%=2.4% in Table I).

E_γ (keV)	I_γ	$K,J^\pi\rightarrow K,J^\pi$	
231	6(1)	$0_s,14^+$	$0_g,14^+$
240	90(17)	$0_g,4^+$	$0_g,2^+$
280	<0.1	$14,14^+$	$5,13$
348	<0.2 [a]	$14,14^+$	$8,14^{(-)}$
351	90(17)	$0_g,6^+$	$0_g,4^+$
363	4(4)	$0_2,8^+$	$0_2,6^+$
408	18(4)	$0_s,14^+$	$0_s,12^+$
418	14(3)	$0_s,12^+$	$0_g,12^+$
430	9(3)	$0_2,10^+$	$0_2,8^+$
434	7(3)	$0_s,12^+$	$0_2,10^+$
440	90(4)	$0_g,8^+$	$0_g,6^+$
445	10(3)		
490	16(4)		
508	90(4)	$0_g,10^+$	$0_g,8^+$
508	<0.2 [b]	$14,14^+$	$6,14(+)$
513	2(1)		
519	12(3)		
541	7(4)	$0_2,10^+$	$0_g,10^+$
558	44(4)	$0_g,12^+$	$0_g,10^+$
596	7(4)	$0_g,14^+$	$0_g,12^+$
619	5(2)	$0_2,8^+$	$0_g,8^+$
624	3(2)	$0_2,12^+$	$0_g,12^+$
632	3(2)		
641	4(4)	$0_2,12^+$	$0_2,10^+$
656	9(3)		
714	33(4)	$14,14^+$	$0_s,14^+$
775	<0.2	$14,14^+$	$7,13^{(-)}$
827	5(2)	$0_s,14^+$	$0_g,14^+$
866	<0.2	$14,14^+$	$4,13^{(-)}$
884	10(3)		
917	13(2)	$14,14^+$	$0_2,12^+$
945	6(3)	$14,14^+$	$0_g,14^+$
1050	7(3)		
1068	5(3)		
1096	3(1)		
1122	$<\sim4$	$14,14^+$	$0_s,12^+$
1541	<2	$14,14^+$	$0_g,12^+$

[a]Intensity was not measurable directly because of the proximity of the strong 351 keV g-band transition. An upper limit was obtained from coincidence spectra of transitions in band 4 with transitions in band 1 above the isomer.

[b]Intensity was not measurable directly because of the proximity of the strong 508 keV g-band transition. An upper limit was obtained from coincidence spectra of transitions in band 8 with transitions in band 1 above the isomer.

The delayed BGO fold parameter proved to be a very powerful tool for investigating the decay of the 35-ns isomer. Although the isomer was populated in this reaction with an intensity of only 2% of the ^{176}W reaction channel, the gamma rays associated with the decay constituted 15% of all

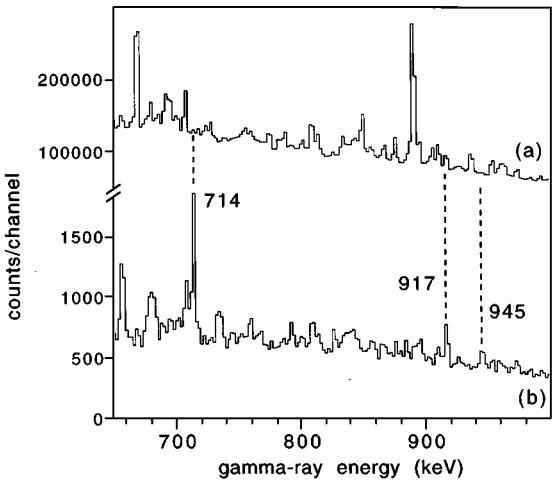

FIG. 5. Demonstration of the sensitivity provided by requiring a coincidence with the delayed firing of four BGO detectors. The transitions from the decay of the 35-ns isomer are not visible in the ungated spectrum (a), but are quite prominent in the spectrum with the coincidence requirement (b).

events with delayed BGO fold $\geqslant 2$ and 45% of those with delayed fold $\geqslant 3$. The power of this method is illustrated by a comparison (Fig. 5) of total projections from the coincidence matrices, both with and without a coincidence requirement that the delayed BGO fold be at least 4. The isomeric decays are not visible above the background without the delayed fold condition, but are clearly visible after the condition is imposed.

In addition to the 35-ns isomer, a second isomer with $t_{1/2} \approx 10$ ns was observed (Fig. 1). The DCO ratios of the transitions depopulating the 35-ns and 10-ns isomers were not measurable, due to the very low intensities involved or deorientation of the nuclear spin during the lifetimes of the isomers, or both. The interlocking pattern of branches in the decay of the 35-ns isomer restricts its spin to $J \leqslant 14$, assuming that no $\lambda = 3$ transitions are involved. For example, if the 917 keV transition were of $E3$ character, its strength would be 17 Weisskopf units (W.u.), while $E3$ transitions with a degree of K forbiddenness ν as low as 1–2 typically have strengths of 10^{-2}–10^{-5} W.u. [2]. Direct decays are observed from the 35-ns isomer to the 14^+ states of the g and s bands, but not to the 12^+ levels. This suggests $J > 13$ for the spin of the isomer, since for $J \leqslant 13$ one would expect stronger branches to the 12^+ states, based on the associated multipolarities and gamma-ray energies. The $M1/E2$ branching ratios for the transitions in the band built on the isomer and the absence of any rotational alignment are also consistent with those expected for the lowest $K = 14$ deformation-aligned configuration, as discussed in Sec. III. Thus, the 35-ns isomer is assigned $J^\pi = 14^+$.

Decay schemes were also constructed for the rotational bands built on the two isomeric bandheads. The technique used to enhance these cascades was the requirement of a delayed coincidence with gamma rays from the decay of the 35-ns isomer, before inspecting the data for coincident transitions with prompt timing. These bands were then investigated further using prompt-prompt coincidence matrices constructed with the requirement of a high delayed BGO fold.

The ordering of the following cascades in the decay of the 35-ns isomer (Fig. 1) could not be determined: 884-656, 445-1096, and 519-1068-512 keV. The ordering of the 316-210-267-355 keV cascade depopulating the 10-ns isomer is based on the intensities of the transitions; the time spectra gated on these transitions are also consistent with this ordering.

A band was also observed built on a high-K state tentatively labeled $K = (13)$. This band (band 9 in Fig. 1) is very prominent in spectra gated on a very high delayed fold and is thus apparently populated partly by the decay of another isomer with even higher spin (Fig. 1). The decay pattern of the $K = (13)$ bandhead could not be mapped out entirely because of its fragmentation into many weak branches; nor could the decay scheme of the very high-spin isomer feeding it be constructed. In contrast to the 14^+ isomer, the decay of the $K = (13)$ state appears to have a half-life too short to measure with electronic timing, and seems to occur both to $K = 0$ states and to the bands with intermediate K values, such as band 8.

III. DISCUSSION

The most important result of this experiment is the observation of highly K-violating transitions in ^{176}W leading directly from the $K = 14$ isomer to the $K = 0$ states in the g, s, and 0_2^+ bands. As noted in Sec. I, there have been several recent observations of transitions with anomalously large values of ΔK in neighboring nuclei in this region. In all these previous cases [3,4,14,16,17], however, the anomalous decays constituted only a small fraction of the total decay of the isomer, while the predominant path of deexcitation was one that followed the usual K-selection rules. An exception is the decay of an isomer in ^{179}W [5], which involves an accidental degeneracy [26,27]. In contrast, the novel feature in ^{176}W is that the *majority* of the decay of the K isomer proceeds through highly K-violating $\Delta K = 14$ transitions, with no observable decay to the many available states with intermediate values of K.

The identification of a $K = 14$ isomer in ^{176}W with multiple K-violating decay branches is especially interesting because similar K-violating decays have recently been studied in the neighboring even-even isotone ^{174}Hf [4]. In addition, as discussed below, we propose a quasiparticle configuration for the isomer in ^{176}W that is the same as that of the isomer in ^{174}Hf. The ability to compare hindrance factors for the decay of K isomers with the same configuration in different nuclei makes this pair of isomers a powerful tool for exploring the mechanisms of highly K-violating decays, since it is possible to examine the systematics of the decays while keeping many of the relevant degrees of freedom constant. The spin and K assignments for the states to which the isomer decays, as well as the levels to which no decay branches are observed, are essential to the discussion of variation of the hindrance factors with K forbiddenness. Therefore, the $K = 0$ and low-K states are discussed first, followed by an analysis of the feeding and decay of the high-K isomers.

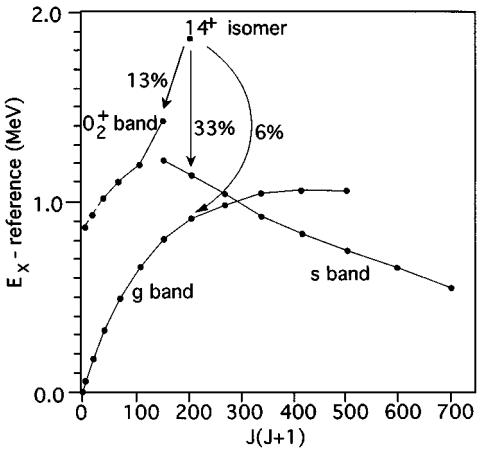

FIG. 6. Excitation energy as a function of $J(J+1)$ for the g, s, and 0_2^+ bands, and the 14^+ isomer in ^{176}W. A rotational band with perfect $J(J+1)$ level spacing would appear on this figure as a straight line. An arbitrary reference value of (9 keV)$\times J(J+1)$ has been subtracted from the excitation energies in order to highlight small deviations from a $J(J+1)$ level spacing, due either to interactions between bands or to other effects such as centrifugal stretching (see text for a detailed discussion). The three arrows show the direct decay paths of the $K=14$ isomer to $K=0$ states, and the associated intensities are given as a fraction of the total strength with which the band is populated.

A. Rotational bands with $K=0$

Figure 6 shows the relative excitation energies of the observed $K=0$ states as a function of $J(J+1)$. From the figure, the presence of three rotational bands with two band crossings is obvious. The nonyrast parts of the g and s bands are easily identified from this figure, and these assignments are confirmed by the deviations from the expected rotational energies in the crossing region, as well as the branching ratios between the two bands. In a simple two-band-mixing scenario, assuming that the interaction matrix element V_{gs} between the two bands is constant with respect to spin, an upper limit of $|V_{gs}|<33$ keV can be stated from the 66-keV difference between the 16_g^+ and 16_s^+ levels, since the energy separation is always greater than $2V_{gs}$. The best source of a lower limit on V_{gs} comes from the interband branching ratios rather than from the energy levels. Such branching ratios have seldom [18] been measurable in previous experiments. In Table III, the measured ratios, $B(E2)_{\rm out}/B(E2)_{\rm in}$ for the $\Delta J=2$ transitions within and between bands are compared to simple two-band-mixing calculations [18] for different values of $|V_{gs}|$, where "out" refers to the out-of-band branch ($g\rightarrow s$ or $s\rightarrow g$) and "in" to the in-band branch ($g\rightarrow g$ or $s\rightarrow s$). The best agreement between calculations and experiment is obtained with $|V_{gs}|\approx 30$–33 keV. The ratios are largest near the crossing of the two bands (between $J=16$ and 18), where the mixing is the greatest. Although the measured values do not all overlap with the calculated numbers within statistical errors, it should be noted that while the ratios span two orders of magnitude, the values calculated under the simple model assumptions mentioned above are within a factor of 5 of the experimental numbers. A value of $|V_{gs}|\approx 32$ keV is adopted below for the discussion of possible mechanisms for the K-violating decays.

TABLE III. Comparison of experimental and calculated branching ratios of out-of-band to in-band stretched $E2$ decays in the s band and g band. The calculated values are given for three different interaction matrix elements V, showing the quality of the fit as a function of V.

Initial state	$B(E2,\text{out})/B(E2,\text{in})$ Expt.	$V=25$ keV	$V=28$ keV	$V=32$ keV
$14^+,s$	0.008(1)	0.002	0.003	0.004
$16^+,s$	0.24(6)	0.11	0.16	0.33
$18^+,s$	1.1(5)	0.05	0.07	0.16
$18^+,g$	1.0(3)	0.05	0.07	0.16

At high spins, a large but gradual increase is observed in the moment of inertia of the g band, as evidenced by the curvature of its E versus $J(J+1)$ trajectory in Fig. 6. Similar effects were observed, e.g., in ^{179}W [19], where the yrast band was also observed to high rotational frequencies. When this type of gradual increase is observed, it has been shown [20–22] that it is not possible, based only on the observed energy levels, to separate the contributions of centrifugal stretching, Coriolis antipairing, and gradual quasiparticle alignments. Calculations using the cranked Nilsson-Strutinsky code of Ref. [23] have been carried out as part of the present work. These calculations indicate that the deformation of the g band increases gradually from $(\epsilon_2)_g=0.24$ in the ground state to $(\epsilon_2)_g=0.29$ at spin 18, and then remains approximately constant from spin 18 through spins greater than 30. (The details of the calculations are given in Sec. III C.) This increase in deformation will lead to an increase in the moment of inertia, with some contribution as well from the Coriolis antipairing effect. It should be noted that no alignment process other than the g-band–s-band crossing is predicted to occur in the range of frequencies being considered. (Alignment processes in this region have been discussed elsewhere [22,24].) No strong centrifugal stretching effect is predicted for the s band, which is expected to maintain a deformation of $(\epsilon_2)_s\approx 0.22$–0.23 for the range of spins observed in this experiment. This is in agreement with the data, since the s band does not show any deviation from $J(J+1)$ level spacing (Fig. 6), such as would be expected if there was significant stretching. Near the g-band–s-band crossing, a rather large difference in deformation is predicted between the s band and g band [$(\epsilon_2)_s=0.22$, $(\epsilon_2)_g=0.29$], consistent with the observation of only a small interaction between the bands. Such deformation changes may be partially responsible for the complicated alignment curves observed in the yrast sequences of the W isotopes [22,24]. It has also been suggested that quadrupole pairing plays a role [25] in the alignment processes in this region, although the effect is predicted to be far more pronounced in the odd-Z systems.

It has been debated [26,27] whether the structure referred to here as the s band might in fact involve two quasineutrons coupled in the novel Fermi-aligned scheme [28], in which the quasineutrons create a state with nonzero $\langle K\rangle=\langle J_z\rangle$, as well as a nonzero rotational alignment $\langle J_x\rangle$. This coupling scheme is predicted to arise from a balance between the mean field and the Coriolis force, and is stable for certain

ranges of values of the rotational frequency, pair gap, and Fermi level. This coupling scheme, however, cannot apply to the band presently being discussed for the following reason. The band shows a nearly perfect pattern of $J(J+1)$ level spacings (Fig. 6) from spin $12\hbar$ to spin $26\hbar$, implying a constant rotational alignment. Thus, only one coupling scheme is involved in this range of spins. Since, even in the most favorable cases, the Fermi-aligned coupling scheme is not predicted [28] to be stable at rotational frequencies as high as those observed here ($\omega > 0.35$ MeV), the entire sequence of states is assigned to a rotation-aligned configuration ("*s* band"), with $\langle K \rangle = 0$.

A third band populated by the decay of the isomer is assigned $K=0$. It is identified as the band structure built on the first excited 0^+ state, and labeled as the 0_2^+ band, based on the following observations: (a) In the region where the 0_2^+ band crosses the *s* band, the measured perturbations of the 12^+ level energies and the interband branching ratios give $|V_{0_2^+,s}| \sim 30$–110 keV for the interaction matrix element. (Sufficient data for a more detailed calculation such as the one performed above for $|V_{gs}|$ are not available.) An interaction this large would be quite anomalous for bands with different K values. (b) No signature partner band is observed in the data. (c) The electromagnetic transitions to the *g* band are fairly strong [$B(M1) \sim 0.02$ W.u., assuming a mixing ratio of $\delta = 0$] compared to those normally seen [2] for K-violating transitions. (d) Although the depopulation of the band at low spins is too sudden to allow the observation of levels with $J<6$ in these data, two states in ^{176}W have been observed (at 929 and 1117 keV) in the radioactive decay of the 3^+ state in ^{176}Re [29], which form a clear continuation of the $J(J+1)$ pattern of excitation energies (see Fig. 6, where these levels have been included). Furthermore, the levels from 2^+ to 10^+ of the 0_2^+ band in ^{176}W are nearly identical (gamma-ray energies differing by <8 keV) to the corresponding levels of the 0_2^+ band in ^{178}W [7], which has been observed down to the $K=0$ bandhead. The $\ln ft$ values are very similar ($\ln ft = 6.7$ and 6.9, respectively [29,30]) for population of the corresponding 2^+ states in ^{176}W and ^{178}W from the ^{176}Re and ^{178}Re β decays.

The observation of the crossing between the *s* band and the 0_2^+ band is noteworthy, since it has only been observed in a few cases [18,31,32]. The band built on the first excited 0^+ state is often labeled as the β-vibrational or "β band." The extrapolated bandhead energy of 0.9 MeV is considerably lower than that expected for a two-quasiparticle state, but attempts to associate such states in this region with simple collective modes like β vibrations or pairing vibrations have failed to reproduce the available data on electromagnetic and particle-transfer matrix elements [33–36]. We therefore avoid the label "β band" in this paper. The measurement of the interaction $V_{0_2^+,s}$ in this work may test future theoretical descriptions of these low-lying excitations.

B. States with intermediate values of *K*

A large number of intermediate-K states is observed in this experiment (bands 3–8 in Fig. 1), and most of these can be assigned 2qp configurations with some confidence. In this section, we discuss the structures of these states, and compare their properties with the results of cranked Woods-Saxon calculations performed using the computer code and the "universal" parameters described in Ref. [37]. The pair gaps were extracted from the odd-even mass differences as in Ref. [42], multiplied by 0.9 as suggested in Ref. [43]. This results in values of $\Delta_p = 0.92$ MeV and $\Delta_n = 0.83$ MeV. Cranking calculations can only determine angular momenta and Routhians relative to some additive reference. We have chosen as the reference a function $\mathfrak{I} = \mathfrak{I}_0 + \mathfrak{I}_1 \omega^2$, with $\mathfrak{I}_0 = 43\hbar^2$ MeV^{-1} and $\mathfrak{I}_1 = 80\hbar^4$ MeV^{-3} fitted to the moment of inertia of band 6 as a function of rotational frequency, because this band is observed over a large range of rotational frequencies.

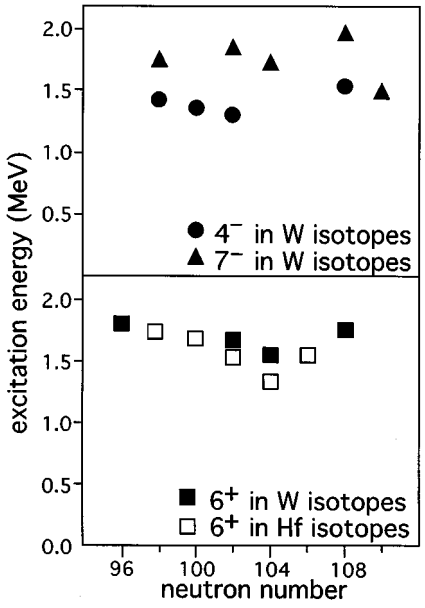

FIG. 7. Systematics of two-quasiparticle states observed experimentally in the W and Hf isotopes.

Bands 3 and 4 require a short preface since it is not entirely clear that 2qp assignments are appropriate for these bands. Based on previous data, it had been suggested [10] that these sequences might correspond to two of the four members of the octupole-vibrational multiplet with $K^\pi = 0^-, 1^-, 2^-, 3^-$. Such an interpretation would require the existence of bandheads with $K<4$, which might not have been observed in previous experiments purely because of the early depopulation of these bands into the *g* band. The present, more sensitive experiment has, however, failed to reveal any further in-band transitions leading to bandheads with $K<4$, calling the vibrational interpretation into question. As shown below, many of the characteristics of these bands can be understood naturally if they are the two signature partners of a two-quasiproton band with $K=4$. We will briefly note below some of the successes and failures of such a description.

A first step in classifying the intermediate-K bandheads as two-quasiproton (π^2) or two-quasineutron (ν^2) states is to examine the systematics of the bandhead energies in nearby nuclei (Fig. 7). The $K=4^-$ and 7^- states occur at approximately constant excitation energies in the W isotopes with $A=172$–184, suggesting that they are π^2 states. The energies of the 6^+ states in the Hf isotopes show evidence of a minimum near $N=104$; this is in agreement with calcula-

TABLE IV. Configurations assigned to intermediate-K bandheads, and comparison of experimental and calculated bandhead energies.

K^π	Configuration	E_x (expt.) (MeV)	E_x (theory) (MeV)
4^-	$\pi\ 1/2^-[541] \otimes \pi\ 7/2^+[404]$	1.301	2.0
7^-	$\pi\ 9/2^-[514] \otimes \pi\ 5/2^+[402]$	1.857	1.9
8^-	$\pi\ 9/2^-[514] \otimes \pi\ 7/2^+[404]$	1.972	1.9
6^+	$\nu\ 5/2^-[512] \otimes \nu\ 7/2^-[514]$	1.656	1.9

tions of the quasineutron states (see below), which show that the configuration $\nu\ 5/2^-[512] \otimes \nu\ 7/2^-[514]$ should be favored in this vicinity, rather than π^2 configurations. (Less extensive data are available for the 6^+ states in the W isotopes.) Both ν^2 and π^2 states with $K^\pi = 8^-$ have been observed in the Hf-W region, but for ^{176}W the π^2 state is predicted to be much lower in energy than the ν^2 state based on the present calculations. Given these inferences regarding the π^2 and ν^2 characters of the states, the configurations are unambiguously determined by the available combinations of Ω values, as supported both by the present Woods-Saxon calculations and the observed one-quasiparticle states in the neighboring odd-A nuclei. The predicted excitation energies are compared with experiment in Table IV. The agreement of the calculated and measured excitation energies is satisfactory, except in the case of the $4^{(-)}$ state.

Figure 8 compares the experimental 2qp Routhians with the calculated ones. The slopes of the observed Routhians are well reproduced, as are the relative energies of the 6^+,7^-, and 8^- Routhians. While the two 4^- Routhians are calculated to be considerably higher in energy compared to experiment, they show the correct energies relative to one another as well as the correct slopes and alignment behavior. The calculations predict the excitation energy of the 6^+ intrinsic state to be lower and the signature splitting of the 4^- Routhians to be larger than the experimental observations.

No attempt is made here to discuss band 7 in detail, since its parity and K are unknown.

C. High-K states

In the following discussion, the data for the high-K states are compared with the results of cranking calculations. The Woods-Saxon potential, as described above for the intermediate-K, 2qp states, is used wherever possible because of its somewhat better description of the structure of the quasiparticle levels. The modified harmonic oscillator (Nilsson) model was used, however, for the calculation of potential energy surfaces in Sec. IV, since a computer code was available [23] which could transform the calculation from the rotating frame into the laboratory frame. This allowed potential energy surfaces to be constructed for a fixed value of $\langle J_x \rangle$ rather than for a fixed rotational frequency. For these calculations, described in more detail below, the Nilsson parameters of Ref. [38] were used.

To understand the unusual pattern of decay of the 14^+ isomer, it is important to analyze both the decay of the isomer and the rotational band built on it in order to obtain as

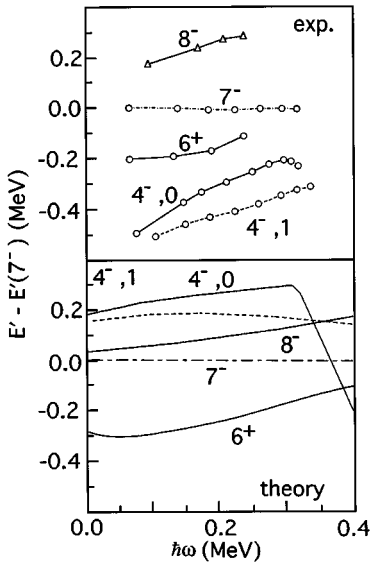

FIG. 8. Comparison of observed and calculated two-quasiparticle Routhians in ^{176}W. Each band is labeled with the quantum numbers K^π or K^π,α.

many clues as possible regarding its underlying structure. Both the Woods-Saxon and Nilsson calculations show that based on the Ω values of the states lying near the Fermi surface, a state with a value of K this large cannot be constructed from the angular momenta of only two quasiparticles. The 14^+ isomer is therefore most likely to be a 4qp state, since 6qp states are not predicted to occur this low in energy. Band 1, the band built on the isomer, is composed of two signature partners with no signature splitting, implying that no $\Omega = 1/2$ orbitals are occupied.

Band 1 is observed up to the rotational frequencies where the $i_{13/2}$ neutron rotational alignment occurs in the yrast cascade, and neither signature partner shows any sign of rotational alignment. This strongly suggests that the $i_{13/2}$ alignment is blocked by the intrinsic configuration.

The 4qp configuration predicted by Woods-Saxon calculations to lie closest to the yrast line is

$$K^\pi = 14^+, \pi 7/2^+[404] \otimes \pi 9/2^-[514] \otimes \nu 7/2^+[633] \otimes \nu 5/2^-[512].$$

The two other low-lying 4qp configurations for a 14^+ state are

$$\pi 7/2^+[404] \otimes \pi 5/2^+[402] \otimes \nu 7/2^+[633] \otimes \nu 9/2^+[624]$$

and

$$\nu 7/2^+[633] \otimes \nu 5/2^-[512] \otimes \nu 7/2^-[514] \otimes \nu 9/2^+[624].$$

The first is calculated to lie at an excitation energy of 3.6 MeV, while both the others lie 400 keV higher at an excitation energy of 4.0 MeV. The first configuration seems to be the most logical choice based on excitation energies alone, since the lowest-lying 14^+ is expected to be the most strongly populated in fusion-evaporation reactions. The observed value of 3.746 MeV is also in closest agreement with the calculated value of 3.6 MeV.

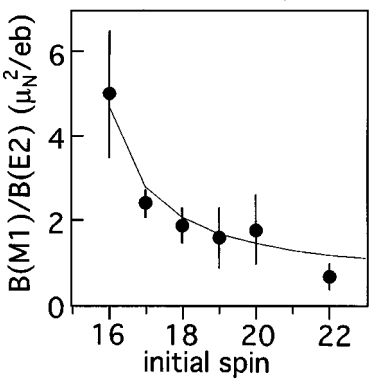

FIG. 9. Comparison of measured (points) and calculated (line) $B(M1)/B(E2)$ ratios in band 1, the band built on the 35-ns isomer in ^{176}W (see text).

In addition, the observed $B(M1)/B(E2)$ branching ratios agree very well (Fig. 9) with those calculated according to the strong-coupling formulas of Ref. [39], using quasiparticle states with the above Nilsson quantum numbers and spin g factors equal to 60% of their free-space values. This configuration has a neutron $i_{13/2}$ orbital occupied, consistent with the absence of rotational alignment.

The spectroscopic information for band 9 (Fig. 1) is rather incomplete. A comparison of its gamma-ray energies with those of the band built on the 35-ns isomer (band 1) suggests a spin of roughly 13. The Woods-Saxon calculations predict a near-yrast state with the configuration $K^\pi = 13^+$, $\pi\ 5/2^+[402] \otimes \pi\ 9/2^-[514] \otimes \nu\ 7/2^+[633] \otimes \nu\ 5/2^-[512]$. The $B(M1)/B(E2)$ data for this band are not very precise, but seem to be consistent with those calculated for this configuration and are higher by an order of magnitude than those of band 1.

Little can be said regarding the configuration of band 2, since the spin and parity of the 10-ns isomer, on which the band is built, are unknown.

D. Summary of data on the decay of the high-*K* states

The most striking observation in this experiment is that the decay of the 14^+ isomer deviates completely from the normal pattern of decay of a K isomer. The majority (52%) of the decay proceeds directly to $K=0$ states, and no branches of any detectable strength were found to the states with intermediate K values, even though many such levels are available, as shown above. This is all the more remarkable since a $K=14$ isomer with the same quasiparticle assignment has also been observed in the neighboring even-even isotone ^{174}Hf at $E_x = 3.312$ MeV [4,14,15], but in ^{174}Hf the highly K-violating branch represents only a small fraction ($\sim 2\%$) of the total decay. Despite these very different patterns of decay, the bands built on the two isomeric states exhibit similar properties. Their moments of inertia are similar ($\mathfrak{I}^{(2)} = 66$ and 63 $\hbar^2$/MeV for ^{176}W and ^{174}Hf, respectively, near their bandheads), and neither exhibits any rotational alignment at the frequency at which the g and s bands cross.

Since detailed data are available on the half-lives and branching ratios for the anomalous decays of the $K=14$ states with identical quasiparticle assignments in ^{176}W and ^{174}Hf, both absolute and reduced hindrance factors ($f = F^{1/\nu}$) for the $\Delta K = 14$ transitions in these two nuclei are compared in Table V. (Transitions have been included in the table only if they are significant at the two-sigma level.) Although the differences between the reduced hindrance factors of the two nuclei may appear small, they represent very large changes in the absolute hindrance factors. For the decays of the 14^+ states to the g bands in ^{176}W and ^{174}Hf, for example, the absolute hindrance factors differ by more than two orders of magnitude. In the following section, the focus is on trying to understand this large difference in absolute hindrance factors.

IV. CALCULATION FOR DECAYS OF HIGH-*K* ISOMERS

Since the first observations [3–5] of gamma-ray transitions between states with large values of ΔK but anomalously low hindrances compared to the usual K-selection rules, it has become necessary to reevaluate old assumptions about K violation, as one would like to understand the mechanism responsible for these exotic decays. Since the decays arise from small-probability fluctuations in the K quantum number, it is not possible to gain direct insight into the decay mechanisms by measuring quantities such as excitation energies or electromagnetic moments and transition rates. At present, the mechanisms of K violation can only be addressed by comparing the K-violating transition strengths with theoretical calculations.

In this section, the focus is on understanding why differences of several orders of magnitude exist between the strengths of the $\Delta K = 14$ transitions in ^{176}W and ^{174}Hf. As discussed in Sec. I, two suggested mechanisms that might be responsible for coupling states with different values of K are

TABLE V. Hindrance factors in the nuclei ^{176}W and ^{174}Hf for decays of 14^+ isomers directly to states with $K=0$. As defined in Sec. I, F is the hindrance factor and f is the hindrance factor per degree of K forbiddenness.

Final state	ν	Branching ratio (%) ^{176}W	Branching ratio (%) ^{174}Hf	F ^{176}W	F ^{174}Hf	f ^{176}W	f ^{174}Hf
$g,14^+$	13	6(3)	1.04(6)	2.0×10^7	5.6×10^9	3.6	5.6
$g,12^+$	12	<2	0.27(12)	$>6.0\times10^5$	5.0×10^8	>3.2	5.3
$s,14^+$	13	33(4)		8.0×10^5		3.0	
$s,12^+$	12	<4	0.71(8)	$>1.2\times10^5$	5.2×10^6	>2.9	(3.6)
$0_2^+,12^+$	12	13(2)	0.59(14)	8.0×10^3	2.4×10^7	2.3	4.1

γ tunneling [3,6] and Coriolis mixing [4]. The Coriolis force mixes wave functions corresponding to the same shape but oriented differently with respect to the angular momentum vector. In contrast, γ tunneling involves large-amplitude collective motion in which the shape of the nucleus changes.

The distinction between these two modes of K mixing can be tested empirically: Coriolis mixing should manifest itself in systematic variations in K mixing as a function of configuration and rotational frequency, while γ-tunneling models predict that K-violating decays should show strong variations in strength as a function of the height and shape of the barrier in the potential energy surface. Both concepts are discussed below in light of the present data.

A. Testing predictions of Coriolis mixing

As described above, an explanation previously proposed to account for the K-violating decays in ^{174}Hf [4] associates a change in Coriolis mixing at high spins with a change in the structure of the yrast states from g-band to s-band configurations. The mean K value of the s-band levels is zero, but because the two quasineutrons are aligned perpendicular to the symmetry axis, admixtures of various K values are to be expected in the s-band wave function, with values of K ranging from 0 to approximately $\pm K_{\max}$, where $K_{\max}^2 = j_{\max}^2 - i^2$. Here, $j_{\max}$ is the maximum spin to which the two neutrons can be coupled subject to the Pauli exclusion principle and i is their rotational alignment. The alignments of the s bands in ^{176}W and ^{174}Hf extracted from the data are 8.7 $\hbar$ and 6.0$\hbar$, respectively, leading to $K_{\max} = 8.3$ and 10.4. [We use $j_{\max}^2$, rather than $j_{\max}(j_{\max}+1)$, since this is only an approximate treatment.] The previously observed highly K-violating decays are then ascribed to Coriolis mixing, with essentially normal values of the hindrance per degree of K forbiddenness, i.e., $f \sim 100$, but with a smaller degree of K violation, $\nu' = \nu - K_{\max}$. Although decays are also observed to the g-band states, such decays are attributed in this model [4] to mixing of the g- and s-band configurations in the band-crossing region, so that the hindrance factors should be approximately $F = f^{\nu'}/(|\langle\Psi|s\rangle|^2 \times |\langle s|K_{\max}\rangle|^2)$. Here, $|\langle s|K_{\max}\rangle|^2$ is the squared amplitude of the part of the pure s-band wave function having $K = K_{\max}$, and $|\langle\Psi|s\rangle|^2$ is the squared amplitude of the s-band configuration in the wave function of the state in question, as calculated in Sec. III.

The model predicts a strong correlation between the hindrance factor and the amount of s-band admixture in the final state. The smaller value of $K_{\max}$ in ^{176}W should also contribute to increased hindrance factors relative to those in ^{174}Hf. Figure 10 presents a test of the predictions of this model for the two 14^+ isomers in ^{174}Hf and ^{176}W. Although the hypothesis was a reasonable one to account for the ^{174}Hf data, the addition of the ^{176}W data to the figure reveals that there is essentially no correlation between the s-band admixture and the hindrance factors. Furthermore, the hindrance factors in ^{176}W are orders of magnitude too low, even with the most drastic assumption of 100% admixture of $K = K_{\max}$ in the s-band states. This is undoubtedly a very schematic treatment of Coriolis mixing; the objective was not to calculate the effect, but simply to search for the expected trends in the data and to evaluate whether the orders of magnitude were in the right range. The lack of correlation between the hindrance factors and the s-band admixtures, however, seems very difficult to explain in any model of Coriolis mixing.

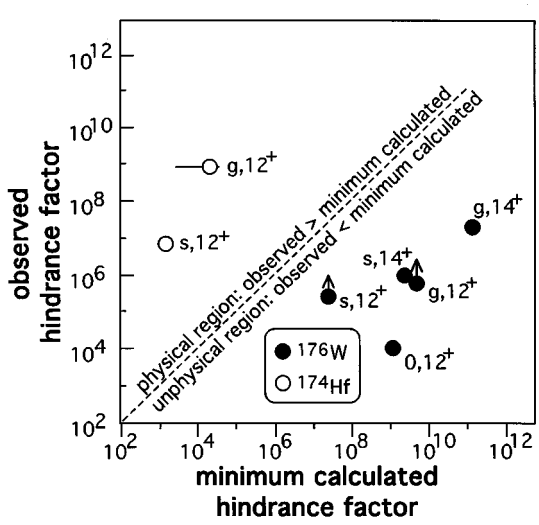

FIG. 10. Comparison of the Coriolis mixing calculations with experiment. The x axis shows the minimum calculated hindrance factor, under the extreme assumption that 100% of the s band wave function has $K = K_{\max}$ (see text). The arrows on the two data points for ^{176}W indicate an experimental upper limit on the corresponding branching ratios. The dashed line represents the assumption that the hindrance factors are as small as possible in the context of the model, and thus data points lying below this line are unphysical.

B. Calculations of γ tunneling

The failure of the Coriolis mixing picture leads one to consider a possible interpretation of these decays in terms of a γ-tunneling picture. The mechanism is schematically illustrated in Fig. 11. Dynamic motion in the shape degrees of freedom of nuclei is often very difficult to describe theoretically, as small-amplitude shape vibrations are usually coupled strongly to the single-particle degrees of freedom. Tunneling processes, therefore, could be extremely important, because they represent a possible simplification of the dynamics. When a nucleus tunnels through a classically forbidden region along a path parametrized by a deformation γ, the wave function is attenuated exponentially, falling off by $1/e$ over a distance $\delta\gamma \propto (V - E_0)^{-1/2}$, where E_0 is the energy eigenvalue of the state, and the potential $V(\gamma)$ is defined as the minimum adiabatic value of the energy at any value of γ. To give some perspective, it is worth noting that

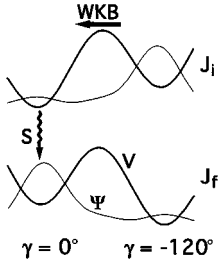

FIG. 11. Schematic representation of the γ-tunneling model. The thick lines depict the potential energy as a function of γ, while the thin lines illustrate the wave function.

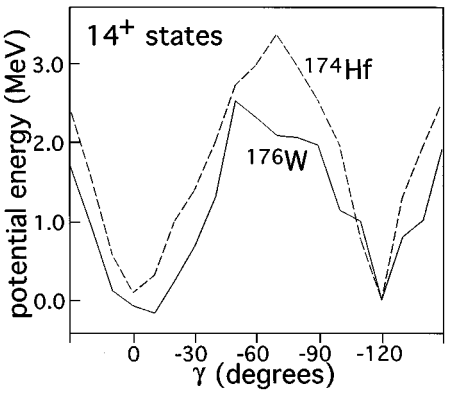

FIG. 12. Calculated potential energy curves for ^{176}W and ^{174}Hf as functions of γ deformation for positive parity and $\langle J_x \rangle = 14$.

even when the decay of a K isomer occurs with an abnormally low hindrance, the hindrance factor F is still on the order of 10^4–10^6 or larger [3–5]. Thus, if tunneling is responsible for these decays, the attenuation is extremely severe. Any motion through nonoptimal single-particle configurations with $E > V$ should, therefore, be strongly attenuated, with the attenuation length reduced to $\delta\gamma \propto (E - E_0)^{-1/2}$. Tunneling processes may be the only type of collective nuclear motion other than rotation for which an adiabatic approximation is justified. For an adiabatic quantum-mechanical tunneling process, the only quantities needed to calculate the tunneling probability are the potential V and the inertial parameter D, which corresponds to the mass in the Schrödinger equation and is discussed in more detail below.

In the present work, the potential energy has been calculated as a function of γ for the $K = 14$ isomers in ^{174}Hf and ^{176}W with the cranked Nilsson-Strutinsky method, using the computer code described in Ref. [23]. In these calculations, the deformation parameters ϵ_2 and ϵ_4, as well as the static pair gaps Δ_p and Δ_n, were all varied self-consistently; i.e., the γ-tunneling path is assumed to be the path of steepest ascent to the saddle point and steepest descent from the saddle point. The cranking frequency was varied to provide a constant value of $\langle J_x \rangle$, and particle-number projection was employed. A step size of 10° was used for γ. Considerable variation was found in ϵ_4 as a function of γ, with values of ϵ_4 ranging from 0.00 to 0.05, and it was found that a proper self-consistent variation of ϵ_4 was necessary for an accurate determination of the potential energy surfaces. The parameters ϵ_2, Δ_n, and Δ_p showed variations as functions of γ, but remained within about 10% of their average values. The calculated potential energy curves are shown in Fig. 12. A summary of some of the calculated parameters is given in Table VI.

In an adiabatic model, the information on the dynamics is contained in the inertial parameter. At present, the dynamics are not understood well enough to allow an accurate calculation of this quantity from first principles. One fact that seems to emerge from all microscopic approaches [6,40] is that superfluidity in nuclei has an important effect on the inertial parameters. Another approach is to take a phenomenological functional form for the inertial parameter and to fit adjustable parameters to the available information on properties of nuclei. The results of such an approach [41] fall within the range of values calculated from the microscopic methods. It is worth noting, however, that the starting point for such a fit is the observed transition rates for tunneling processes as observed in the decays of fission isomers [41]. From this point of view, experiments involving tunneling processes could directly measure the inertial parameters. Such a program might be a reasonable one to pursue for K isomers in the long run, but first it must be established whether a γ-tunneling approach can provide a reasonable description of the data. This is the more modest goal of this paper. As is explained in more detail below, the calculations factor out most of the effect of the inertial parameter and the final results are inspected to see whether they can approximately reproduce the data for a reasonable choice of the inertial parameter.

The WKB approximation for the tunneling probability is $T = \exp[-2\hbar^{-1}\int\sqrt{2D(V - E_{\rm ZP})}d\gamma]$ where $E_{\rm ZP}$ is the zero-point energy, i.e., the eigenvalue of the Schrödinger equation, and D and V are defined as above. The tunneling probability T represents the squared amplitude of the part of the wave function localized in the potential well around $\gamma = 0°$, which is interpreted as the admixture of the $K = 0$, $J = 14$ component in the wave function of the $J = 14$ state (which has predominantly $K = 14$). The hindrance factor for the K-violating transition is calculated as $F^{\rm calc} = 1/TS$, which can be compared with the measured quantity $F^{\rm expt} = t_{1/2}/t_{1/2}^{W}$, as defined in Sec. I. Here, the absolute normalization of the transition rate is determined via the constant S. The strengths of unhindered $M1$ transitions (i.e., those with ΔK less than λ, the multipolarity of the phonon) typically cover a range of 0.03–0.3 W.u. [2], and the corresponding range of S is depicted as a horizontal bar in the figures below, showing the final results of the calculations. In the case of $E2$ transitions, the model ascribes the decay of the isomer to mixing of the $K = 14$ wave function with a $K = 0$, $J^\pi = 14^+$ wave function such as that of the $J^\pi = 14^+$ member of the g band. This admixture then allows an $E2$ decay to occur to the $K = 0$, $J^\pi = 12^+$ state. We have chosen a range of 10–100 W.u. for unhindered stengths of such allowed $E2$ transitions. The final calculated transition rates, which incorporate the factor $1/T$, are, of course, much smaller.

TABLE VI. Calculated barrier, shape, and dynamical parameters used in the γ-tunneling model for the 14^+ states. V_B is defined as $V(\gamma = \gamma_B) - V(\gamma = -120°)$, where γ_B refers to the saddle point.

	V_B (MeV)	ϵ_2 ($\gamma = -120°$)	ϵ_2 ($\gamma = \gamma_B$)	ϵ_2 ($\gamma = 0$)	$E_{\rm ZP}$ (MeV)	$\epsilon_2/\epsilon_2(0)$	$[R_\Delta/R_\Delta(0)]^{1/2}$
^{174}Hf	3.4	0.26	0.25	0.26	0.53	0.96	1.00
^{176}W	2.5	0.25	0.23	0.25	0.43	0.90	0.94

An estimate of the zero-point energy $E_{\rm ZP}$ was obtained by calculating the energy for Gaussian trial wave functions $\Psi(\gamma)$, with the Gaussian width used as a variational parameter. Since the isomers are $\sim$1 MeV higher in energy than the yrast levels with the same spin, it is assumed that the dominant contribution to the decay comes from tunneling from the minimum at $\gamma=-120°$ to the one at $\gamma=0°$ (giving low-K admixtures in the initial state), rather than from tunneling in the opposite direction (which would result in high-K admixtures in the final state).

As explained above, the philosophy adopted here is one of extracting the inertial parameter D and comparing it with various *a priori* estimates. There are two ways in which D, which is assumed to remain constant with γ, affects the calculated hindrance factors. The more important one is the explicit dependence of the tunneling probability on D. In addition, the zero-point energy also depends on D ($E_{\rm ZP}\sim\sqrt{D}$ for a harmonic well). Neglecting the latter for the moment, simple algebra yields $\ln F^{\rm calc}=(\sqrt{D}\times A)-\ln S$, where the quantity $A=2\hbar^{-1}\int\sqrt{2(V-E_{\rm ZP})}d\gamma$ is independent of D. In other words, in a log-log diagram of $F^{\rm expt}$ vs $F^{\rm calc}$, the slope is proportional to $D^{1/2}$ and a change in S shifts the data points horizontally. The slope equals 1 for the correct value of D, and this is essentially the method used here to extract values of D from the data, although the minor dependence of $E_{\rm ZP}$ on D has also been taken into account, as shown below.

To describe consistently the variations of the tunneling probabilities from nucleus to nucleus, it is necessary to recognize that a systematic variation in the inertial parameter is to be expected, depending on actual deformations and pair gaps. Various microscopic models predict a variation of the inertial parameter proportional to Δ^{-2} [6,40], and variation with the deformation is expected [41] to result in an ϵ_2^2 dependence. We have therefore made the following modification: $\ln F^{\rm calc}\rightarrow\ln F^{\rm calc}\times f(\epsilon,\Delta)$, where $f(\epsilon,\Delta)=(\epsilon_2/\epsilon_2^{(0)})\times(R_\Delta/R_\Delta^{(0)})^{1/2}$ and R_Δ is an appropriately chosen function of Δ_p and Δ_n. The value of $\epsilon_2^{(0)}$ was fixed at 0.25. Since the inertial parameter depends on both pairing gaps Δ_p and Δ_n, a functional form for R_Δ must be chosen. Motivated by the method used in Ref. [6] to calculate the inertial parameter, the expression $R_\Delta=\Sigma G_i\Delta_i^{-2}/\Sigma G_i$ was chosen, where the index i refers to neutrons and protons, and the pairing strengths are $G_n=(18\ {\rm MeV})/A$ and $G_p=(21\ {\rm MeV})/A$ [6]. (It should be noted, however, that other authors [40] have proposed somewhat different functional forms for this dependence on the pair gaps.) Since the calculations do not show very large variations in the pair gaps as a function of γ, the pair gaps used in the tunneling calculations have been determined simply from the odd-even mass differences [42]. The quadrupole deformations ϵ_2 have been taken from the calculated values at the saddle point. The reference value of R_Δ (denoted as $R_\Delta^{(0)}$) was fixed at 1.21 MeV^{-2}, the value for ^{174}Hf. A summary of the dynamical quantities for the 14^+ states is included in Table VI. It should be emphasized that since the model of tunneling is entirely adiabatic, no attempt was made to take into account any difference in tunneling for different configurations with the same spin and parity.

Before comparing theory and experiment for the 14^+ isomers, the model was tested on a series of 6^+ isomers in nuclei in this region. Data are available for a large sample of nuclei, all having 6^+ isomers decaying through transitions of the same $E2$ multipolarity, and the decays to the 4^+ levels of the $(K=0)$ ground-state bands represent an excellent test of the predictive power of the model. The results of the calculations, shown in Fig. 13, exhibit a clear correlation between the calculated and observed hindrance factors. The correlation between $F^{\rm expt}$ and $F^{\rm calc}$ is not significantly affected, for example, by the specific choice of the functional form of R_Δ, although the slope of the line is subject to some change, introducing some ambiguity in extracting a value of D. Subject to this uncertainty, the inertial parameter required to fit the data is $D\sim 30\hbar^2$ MeV^{-1} rad^{-2}, which is of the right order of magnitude compared to a previous estimate of $\sim 13\hbar^2$ MeV^{-1} rad^{-2} at zero spin [41].

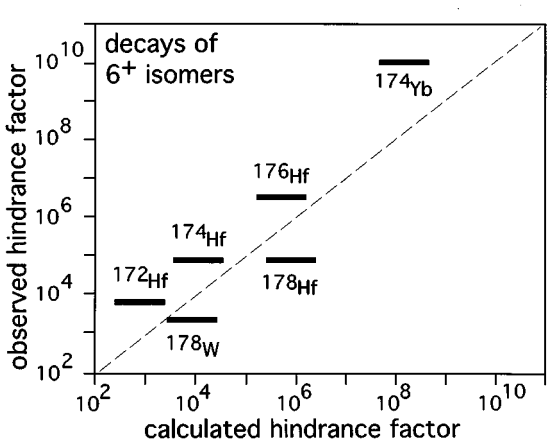

FIG. 13. Test of the γ-tunneling interpretation as applied to $K=6$ states in the rare-earth region. The dashed line is obtained for a value of the inertial parameter $D=30\hbar^2$ MeV^{-1} rad^{-2}. The width of each data point indicates the range given in the text for the unhindered strength S.

Returning to the $K=14$ isomers, the results for ^{176}W and ^{174}Hf are shown in Fig. 14. As in the case of the 6^+ isomers,

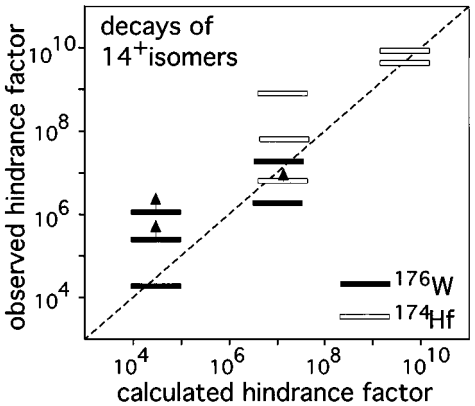

FIG. 14. Test of γ tunneling for the 14^+ isomers. The dashed line in this case is for an inertial parameter $D=60\hbar^2$ MeV^{-1} rad^{-2}. As in Fig. 13, the width of each data point indicates the range given in the text for the unhindered strength S. The data points with arrows pointing upwards represent lower limits on the hindrance factors.

the tunneling calculations reproduce the variations of the hindrance factors. The extracted inertial parameter is $D \sim 60\hbar^2$ MeV^{-1} rad^{-2}. Remembering that the absolute hindrance factors span many orders of magnitude, it is encouraging that data on the 6^+ and 14^+ isomers can be reproduced with values of the D that are of the right order of magnitude compared to the estimate of Ref. [41]. It should be reemphasized that the goal here was not to extract an accurate value of D, but simply to investigate the possibility that systematic variations in the hindrance factors can be understood using a physically acceptable value of D. The fitted value of D is quite sensitive to some of the phenomenological assumptions, such as the form of the function $f(\epsilon,\Delta)$. Nevertheless, the inertial parameter is a quantity of great physical interest, and the results presented here are encouraging as an indication of the future possibilities for extracting information about dynamics from this type of data, provided that appropriate refinements are included in the model. The 6^+ data provide support for the broad predictive power of the model, although these states follow the ordinary pattern of decay of K isomers, and could perhaps be explained in other frameworks. More importantly, the qualitatively new pattern of decay observed for the 14^+ isomer in ^{176}W provides evidence that a new mechanism of decay is being observed, and that the agreement of the calculations with experiment is unlikely to be fortuitous.

An important aspect of the experimental observations in ^{176}W that could not be addressed in the simple γ-tunneling model is the complete absence of decays of the $K=14$ isomer to the intermediate-K states. To address this issue one needs cranking models where the angular momentum vector is not restricted to lie along a principal axis. An obvious next step is to expand the γ-tunneling calculations to include as a second degree of freedom the tilting angle $\vartheta = \arccos[K/\sqrt{J(J+1)}]$, which is the angle between the angular momentum vector and the axis of symmetry. It appears that ^{176}W, in which the ordinary pattern of decay to states of similar K is absent, is an extreme case, in which the γ degree of freedom is dominant. Such a calculation would not only provide a way to evaluate the relative importance of the γ and ϑ degrees of freedom in intermediate cases, but would also allow the calculation of the decays to states with intermediate K, which are outside the model space of principal-axis cranking calculations. The calculation of cranking wave functions at various values of ϑ is a subject of much current theoretical work [44–49].

A schematic method for understanding the fluctuations in the orientation or "tilting" angle ϑ has been suggested recently [50], in which a spectrum of states is calculated near the yrast line, corresponding to a variety of K values. These states are subsequently coupled together with randomly chosen matrix elements. The matrix elements are assumed to vary from zero to $V_{ij}=V_0 f_V^{|K_i-K_j|}$, where V_0 and f_V are phenomenological parameters to be fitted to the data. Matrix elements connecting states with $|K_i-K_j|>1$ are intended to describe the nonaxial shape fluctuations. The hindrance factors thus calculated are mainly sensitive to the level densities.

In order to evaluate the applicability of this model to the present data, we have calculated the spectrum of $J=14$ states

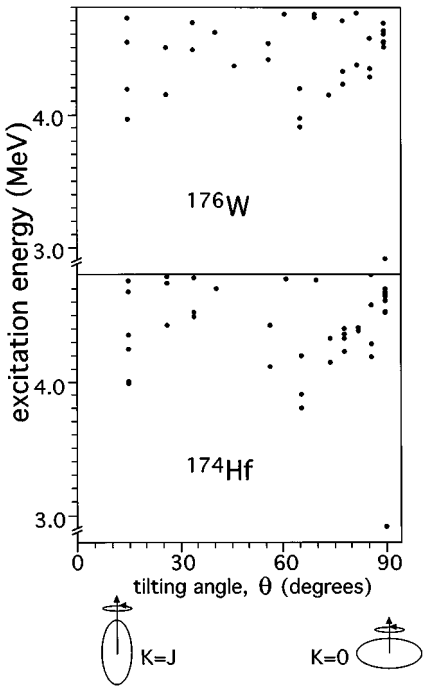

FIG. 15. Excited 14^+ states calculated in ^{176}W and ^{174}Hf as a function of the tilting angle. Note that because of zero-point rotation, states with $K=J$ have tilting angles slightly greater than zero.

located near the yrast line in ^{176}W using the unified model. The intrinsic states came from calculations using the Nilsson model [23], with particle-number projection to avoid the introduction of spurious particle-particle and hole-hole states for configurations involving quasiparticles far from the Fermi level. A deformation of $\epsilon=0.23$ was used, and the pair gaps were adjusted to reproduce the typical energy differences among 0qp, 2qp, and 4qp states. The moments of inertia were taken to be $\Im=36\hbar^2$, $46\hbar^2$, and $56\hbar^2$ MeV^{-1}, for 0qp, 2qp, and 4qp states, respectively. In contrast to the calculations of Ref. [50] where all states were included, only the states with the same spin and parity were considered. Rotational-alignment effects were ignored in these calculations for simplicity, especially since the core rotational frequencies involved are all below the values at which alignments occur and the goal was only to compare the densities of states. The results for ^{174}Hf and ^{176}W are shown in Fig. 15. The density of 14^+ states is essentially the same in both cases. The Fermi level changes by only 0.4 MeV between Hf and W because of the high density of proton levels. Since this change in the Fermi level is significantly less than the pair gap Δ, the quasiparticle energies $\sqrt{(E-\lambda)^2+\Delta^2}$ change very little. For the range of energies shown in the figure, the average density of states for a given value of K is 1.1 MeV^{-1} for ^{176}W and 1.3 MeV^{-1} for ^{174}Hf. Within the perspective of the model, this result implies that orientation fluctuations in ^{176}W should be slightly smaller than those in ^{174}Hf, but the experimental observations are to the contrary. The calculations of Ref. [50] also result consistently in a strong correlation between the hindrance factors and the degrees of K forbiddenness, and such a correlation is not observed in the decay of the isomer in ^{176}W.

It has been suggested [50] that γ tunneling should actually become less competitive at high spin, since the inertial parameter varies with pairing as Δ^{-2} and pairing is weaker at high spins. However, BCS calculations with particle-number projection, such as those carried out here, show only a very slow decrease of Δ. Our fitted values of the inertial parameter D seem to exhibit an increasing trend as a function of spin, but we do not presently consider our method of fitting sufficiently reliable to constitute an experimental measurement of D as a function of spin.

V. CONCLUSIONS

Until the last decade, it appeared that a satisfactory understanding of the systematics of K-violating transitions had been achieved [2], with universal hindrance factors of about 100 per degree of K forbiddenness. More recent data [3,4], including the present work, have now shown that significant deviations from the previously established systematics can occur. In particular, a $K=14$ four-quasiparticle isomer was found in ^{176}W for which these deviations represent the only detectable mode of decay; the usual decay paths, which tend to minimize the degree of K violation, were not observed at all. The decay of this isomer is even more intriguing when compared with the decay of another $K=14$ isomer, with an identical configuration, in the neighboring nucleus ^{174}Hf, where the hindrance factors for similar $\Delta K=14$ transitions are larger by two orders of magnitude. Simple models of Coriolis mixing and γ tunneling were applied in an attempt to account for these observations. It was found that the present results on the decay of $K=14$ isomers cannot be reproduced with simple extensions of the accepted picture of Coriolis mixing. In contrast, a γ-tunneling framework seems to provide a natural explanation for the marked differences between the ^{176}W and ^{174}Hf decays, although the issue of the lack of decay of the ^{176}W isomer to intermediate-K states falls outside the model space of these calculations. The ^{176}W nucleus may have provided the first example of a high-K isomer whose decay is dominated by large-amplitude, nonaxial fluctuations of the nuclear shape. In most nuclei, however, both shape fluctuations and fluctuations in the orientation of the nucleus with respect to the angular momentum vector will be important at moderate spins. Calculations incorporating both degrees of freedom are clearly desirable.

ACKNOWLEDGMENTS

The authors thank J. Greene for the fabrication of the Nd targets, T. Bengtsson and the Warsaw theory group for making their computer codes available to the physics community, and S. Frauendorf for stimulating discussions. This work was supported in part by U.S. DOE Contracts Nos. DE-FG02-91ER-40609, W-31-109-ENG-38, and DE-FG02-94ER40848.

[1] A. Bohr and B.M. Mottelson, *Nuclear Structure* (Benjamin, New York, 1975), Vol. II.
[2] K.E.G. Löbner, Phys. Lett. B **26**, 369 (1968).
[3] P. Chowdhury *et al.*, Nucl. Phys. **A485**, 136 (1988).
[4] P.M. Walker *et al.*, Phys. Rev. Lett. **65**, 416 (1990); N.L. Gjorup, P.M. Walker, G. Sletten, M.A. Bentley, B. Fabricius, and J.F. Sharpey-Schafer, Nucl. Phys. **A582**, 369 (1995).
[5] P.M. Walker *et al.*, Nucl. Phys. **A568**, 397 (1994).
[6] T. Bengtsson, R.A. Broglia, E. Vigezzi, F. Barranco, F. Dönau, and Jing-ye Zhang, Phys. Rev. Lett. **62**, 2448 (1989).
[7] P.C. Sood, D.M. Headly, and R.K. Sheline, At. Data Nucl. Data Tables **47**, 89 (1991).
[8] B. Crowell, P. Chowdhury, D.J. Blumenthal, S.J. Freeman, C.J. Lister, M.P. Carpenter, R. Henry, R.V.F. Janssens, T.L. Khoo, T. Lauritsen, Y. Liang, F. Soramel, and I.G. Bearden, Phys. Rev. Lett. **72**, 1164 (1994).
[9] Danzhao Ye, Ph.D. thesis, University of Notre Dame, 1991.
[10] G.D. Dracoulis, P.M. Walker, and A. Johnson, J. Phys. G **4**, 713 (1978).
[11] I.Y. Lee, C. Baktash, and J.X. Saladin, Phys. Rev. C **29**, 837 (1984).
[12] B. Crowell, Ph.D. thesis, Yale University, 1993.
[13] B. Crowell *et al.* (unpublished).
[14] G. Sletten *et al.*, Nucl. Phys. **A520**, 325c (1990).
[15] P.M. Walker, Phys. Scr. T **5**, 29 (1983).
[16] A. Kramer-Flecken, Ph.D. thesis, University of Bonn, Jülich Report No. Jül-Spez-458, 1988.
[17] A. Kramer-Flecken, T. Morek, R.M. Lieder, W. Gast, G. Hebbinghaus, H.M. Jäger, and W. Urban, Nucl. Instrum. Methods A **275**, 333 (1989).
[18] T.L. Khoo, F.M. Bernthal, J.S. Boyno, and R.A. Warner, Phys. Rev. Lett. **31**, 1146 (1973).
[19] P.M. Walker, G.D. Dracoulis, A.P. Byrne, B. Fabricius, T. Kibédi, and A.E. Stuchberry, Phys. Rev. Lett. **67**, 433 (1991).
[20] R. Bengtsson, in *Proceedings of the XVIII Mikolajki Summer School*, Mikolajki, Poland, 1986, edited by Z. Wilhelmi and G. Szeflinska (Harwood Academic, Chur, Switzerland, 1987), p. 20.
[21] T. Bengtsson, Nucl. Phys. **A520**, 201c (1990).
[22] R. Bengtsson, in *Proceedings of the International Conference on High-Spin Physics and Gamma-Soft Nuclei*, Pittsburgh, 1990, edited by J.X. Saladin, R.A. Sorensen, and C.M. Vincent (World Scientific, Singapore, 1991), p. 289.
[23] T. Bengtsson, Nucl. Phys. **A496**, 56 (1989), and references therein.
[24] F.M. Bernthal, C.L. Dors, B.D. Jeltema, T.L. Khoo, and R.A. Warner, Phys. Lett. **64B**, 147 (1976).
[25] Y. Sun, S. Wen, and D.H. Feng, Phys. Rev. Lett. **72**, 3483 (1994).
[26] P.M. Walker and G.D. Dracoulis, Phys. Rev. Lett. **72**, 3736 (1994).
[27] B. Crowell *et al.*, Phys. Rev. Lett. **72**, 3737 (1994).
[28] S. Frauendorf, Nucl. Phys. **A557**, 259c (1993).
[29] Eh.E. Berlovich, P.P. Vajshnis, V.D. Vitman, R.V. Moroz, and V.K. Tarasov, Probl. Yad. Fid. Kosm. Luchei **7**, 15 (1977).
[30] P.F.A. Goudsmit, J. Konijn, and F.W.N. deBoer, Nucl. Phys. **A151**, 513 (1970).
[31] H.R. Andrews *et al.*, Nucl. Phys. **A219**, 141 (1974).
[32] R.M. Lieder *et al.*, Phys. Lett. **49B**, 161 (1974).

[33] O. Mikoshiba, R.K. Sheline, T. Udagawa, and S. Yoshida, Nucl. Phys. **A101**, 202 (1967).
[34] D.R. Bes and R.A. Broglia, Nucl. Phys. **80**, 289 (1966).
[35] B.L. Birbair, N.A. Voinova, and N.S. Smirnova, Nucl. Phys. **A251**, 169 (1975).
[36] D.G. Burke, G. Lovhoiden, and T.F. Thorsteinsen, Nucl. Phys. **A483**, 221 (1988).
[37] S. Cwiok, J. Dudek, W. Nazarewicz, J. Skalski, and T. Werner, Comput. Phys. Commun. **46**, 379 (1987).
[38] T. Bengtsson and I. Ragnarsson, Nucl. Phys. **A436**, 14 (1985).
[39] F. Dönau and S. Frauendorf, in *Proceedings of the International Conferences on High Angular Momentum Properties of Nuclei*, Oak Ridge, 1982, edited by N.R. Johnson (Harwood Academic, Chur, Switzerland, 1983), p.143.
[40] F. Barranco, G.F. Bertsch, R.A. Broglia, and E. Vigezzi, Nucl. Phys. **A512**, 253 (1990).
[41] P. Möller and J.R. Nix, Nucl. Phys. **A361**, 117 (1981).
[42] A.S. Jensen, P.G. Hansen, and B. Jonson, Nucl. Phys. **A431**, 393 (1984).
[43] R. Wyss *et al.*, Phys. Lett. B **215**, 211 (1988).
[44] S. Frauendorf, in *Contemporary Research Topics in Nuclear Physics*, edited by D.W. Feng, M. Vallieres, M.W. Guidry, and L.L. Riedinger (Plenum, New York, 1982), p. 1.
[45] S. Frauendorf and T. Bengtsson, in *Future Directions in Nuclear Physics with 4π Gamma Detection Systems of the New Generation*, edited by J. Dudek and B. Haas, AIP Conf. Proc. No. 259 (AIP, New York, 1992).
[46] F. Dönau, Nucl. Phys. **A496**, 333 (1989).
[47] F. Dönau, Nucl. Phys. **A520**, 437c (1990).
[48] F. Dönau, Nucl. Phys. **A517**, 125 (1990).
[49] F. Dönau, in *Proceedings of the International Conference on High-Spin Physics and Gamma-Soft Nuclei* [22], p. 66.
[50] S. Frauendorf, in *Proceedings of the International Conference on the Future of Nuclear Spectroscopy*, Crete, 1993, edited by W. Gelletly, C.A. Kalfas, and R. Vlastou (Institute of Nuclear Physics, Athens, Greece, 1994).